2019

The Rhesus Macaque Corticospinal Connectome

Sydney Talmi

The Rhesus Macaque Corticospinal Connectome

A Thesis Presented

By

Sydney Mey Talmi

To the Keck Science Department of Claremont McKenna College, Pitzer College, and Scripps College

In Partial Fulfillment of

The Degree of Bachelor of Arts

Senior Thesis in Neuroscience

December 10, 2018

Table of Contents

Abstract

The corticospinal tract (CST), which carries commands from the cerebral cortex to the spinal cord, is vital to fine motor control. Spinal cord injury (SCI) often damages CST axons, causing loss of motor function, most notably in the hands and legs. Our preliminary work in rats suggests that CST circuitry is complex: neurons whose axons project to the lower cervical spinal cord, which directly controls hand function, also send axon collaterals to other locations in the nervous system and may engage parallel motor systems. To inform research into repair of SCI, we therefore aimed to map the entire projection pattern, or "connectome," of such cervically-projecting CST axons. In this study, we mapped the corticospinal connectome of the Rhesus macaque - an animal model more similar to humans, and therefore more clinically relevant for examining SCI. Comparison of the Rhesus macaque and rat CST connectome, and extrapolation to the human CST connectome, may improve targeting of treatments and rehabilitation after human SCI.

To selectively trace cervically-projecting CST motor axons, a virus encoding a Cre-recombinase-dependent tracer (AAV-DIO-gCOMET) was injected into the hand motor cortex, and a virus encoding Cre-recombinase (AAV-Cre) was injected into the C8 level of the spinal cord. In this intersectional approach, the gCOMET virus infects many neurons in the cortex, but gCOMET expression is not turned on unless the nucleus also contains Cre-recombinase, which must be retrogradely transported from axon terminals in the C8 spinal cord. Thus, gCOMET is only expressed in neurons that project to the C8 spinal cord, and it proceeds to fill the entire neuron, including all axon collaterals. Any gCOMET-labeled axon segments observed in other regions of the nervous system are therefore collaterals of cervically-projecting axons. gCOMET-positive axons were immunohistochemically labeled,

and axon density was quantified using a fluorescence microscope and Fiji/ImageJ software. Specific regions of interest were chosen for analysis because of their known relevance in motor function in humans, and for comparison to results of a similar study in rats. Results in the first monkey have revealed both similarities and differences between the monkey and rodent CST connectome. Analyses of additional monkeys are ongoing. The final results will provide detailed information about differences between rodent and primate CST, will serve as a baseline for examining changes in the CST connectome after SCI, and will provide guidance for studies targeting treatment and functional recovery after SCI.

Introduction

Spinal cord injury is a serious medical problem that currently affects approximately 288,000 people in the United States, impacting about 17,700 new cases each year (National Spinal Cord Injury Statistical Center, 2018). Of people affected by traumatic spinal cord injury, 47.2% suffer from incomplete tetraplegia and 11.5% suffer from complete tetraplegia (National Spinal Cord Injury Statistical Center, 2018), which is associated with the loss of muscle strength and sensation in all four extremities and the torso. Unfortunately, there is currently no treatment that is able to reverse damage and regenerate axons in the adult central nervous system to improve function.

The CST is critical for fine motor function and is therefore a prime target for therapy after SCI. The CST is a pathway made up of upper motor neurons originating from the motor cortices that coordinate the activity of the lower motor neurons in the ventral horn of the spinal cord. These lower motor neurons innervate the muscle fibers of the muscle

intended for movement, making the CST crucial in motor function. Damage to the CST depends on the location of the damage but generally diminishes motor function. Lesioning of higher areas like upper motor neurons may result in paralysis, decreased reflexes, decreased muscle tone due to atrophy, and fasciculations and fibrillations. While lesioning to lower motor neurons may result in weakening, spasticity, and loss of fine voluntary movement. Because the CST is particularly important in distal forelimb movement (such as fine finger function), CST repair could substantially increase independence of the patient if improved (Lang, C. & Schieber, M., 2004).

As observed in a previous study of the rat connectome (Conner, M., Ovruchesky, E., Takashima, Y., Biane, J., Gibbs, D., & Tuskynski, M., manuscript under review), the CST is actually more complex than homogeneous axon projection to the spinal cord. Instead, CST axon collaterals also terminate in other areas of the brain such as the subthalamic nucleus and the thalamus. Understanding the complexity of these collateral projections from the primary motor cortex may allow us to better shape treatment after SCI.

Recent studies have shown promising advancements in SCI treatment by utilizing neuronal progenitor cell grafts implanted into the spinal cord in specifically targeted areas of the CST associated with distal hand function. One of these studies in rats was successful in obtaining results of a surviving human multipotent neural progenitor cell graft in the spinal cord which promoted axonal regeneration and improved skilled forelimb function (Kadoya, K., *et al.*, 2016). Following similar protocol, studies within the Rhesus macaque were unsuccessful in graft survival. However, graft survival was accomplished once immunosuppressant drug levels and growth factor cocktail concentrations were increased, as well as tilting of the operation table immediately after grafting to drain cerebrospinal fluid

from the lesion site. The graft consisted of human multipotent neural progenitor cell graft implanted into the hemisection lesion site at C7 in the Rhesus macaque. Monkeys with surviving grafts exhibited >25% recovery in object manipulation scores in 4 out of the 5 subjects and had significantly greater peak right-hand object manipulation scores than monkeys without grafts (Rosenzweig, E., *et al.*, 2018). This discrepancy in graft survival between the rat and monkey for improvement of distal forelimb function highlights the physiological differences in the two animals, which prompts the necessity of studies in larger animal models for clinical relevance application in humans.

Given the promising breakthrough of graft survival in Rhesus macaque, the next step is specifically targeting regions in the CST with substantial roles in voluntary movement. A study mapping the corticospinal projections associated with distal forelimb control in rats, otherwise known as the rat connectome, provided a preliminary protocol and comparative baseline for subsequent studies in larger animal models (Conner, M., Ovruchesky, E., Takashima, Y., Biane, J., Gibbs, D., & Tuskynski, M., manuscript under review). Similar methods to the rat connectome project were used in this present study to curate a connectome of cervically projecting corticospinal tract motor axon collaterals in the Rhesus macaque. Results may bring to light regions of relevance in motor function, defined by the total sum of innervating axons within the area, which may allow for specific targeting in SCI treatment and functional recovery. These regions of interest from the Rhesus macaque- a facultative bipedal, larger animal model- may more closely represent the areas relevant for human motor function. Therefore, allowing for closer clinical relevance in targeting areas for treatment, as well as providing an established baseline of normal axon density to compare to post SCI for direction of rehabilitation.

Materials and Methods

Subjects

The subject tested was a male Rhesus macaque (Macaca mulatta) raised at the California National Primate Research Center of University of California Davis. All surgical and experimental procedures adhered to the principles outlined by the American Association for the Accreditation of Laboratory Animal Care and were approved by the Institutional Animal Care and Use Committee at the California National Primate Research Center of University of California Davis. The subject had not participated in any previous studies and was sacrificed and perfused at the age of 9 years. Tissue processing was then performed at the Center for Neural Repair at the University of California San Diego.

Corticospinal Tracing

Performed at the University of California Davis, a virus encoding a Cre-recombinase-dependent-tracer (AAVdj-DIO-gCOMET) was injected into the hand motor cortex so that gCOMET anterogradely infected all neurons and axon collaterals projecting from the motor cortex (Fig. 1). A virus encoding Cre-recombinase (AAV-Cre) was injected into the C8 level of the spinal cord, which directly controls hand function. Only neurons with nuclei containing both gCOMET from the motor cortex and AAV-Cre, which is retrogradely transported from the C8 of the spinal cord, has activation of the expression of gCOMET which ensures selective tracing of cervically projecting CST motor axon collaterals.

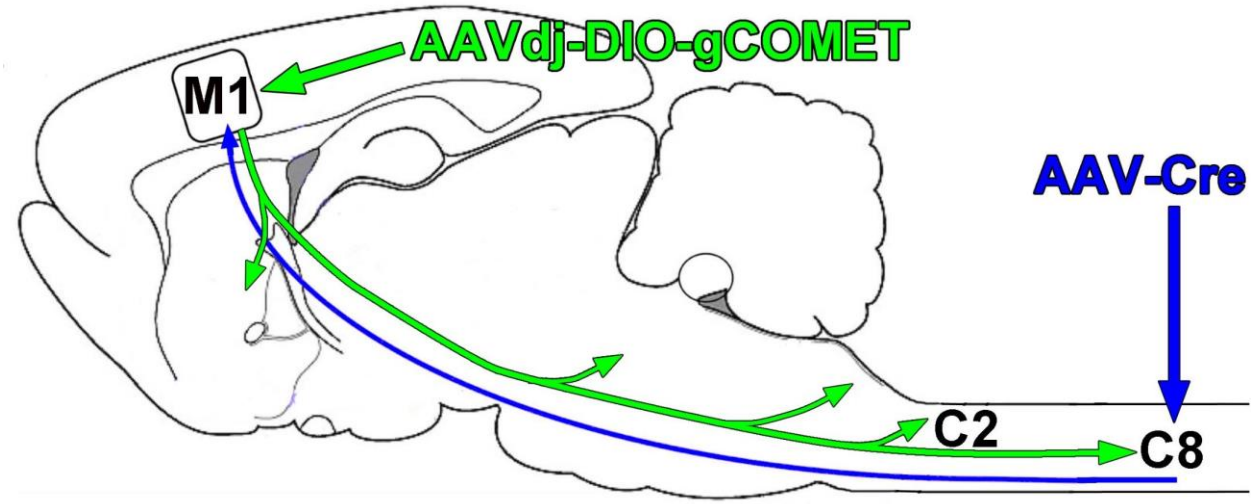

Figure 1.

Intersectional corticospinal tracing method. AAV-Cre, represented in blue, is the virus encoding Cre-recombinase, and the AAVdj-DIO-gCOMET, represented in green is the Cre-recombinase dependent tracer. The AAVdj-DIO-COMET is injected into the hand motor cortex and the AAV-Cre is injected into the C8 of the spinal cord to selectively trace cervically projecting corticospinal tract motor axons collaterals (Rosenzweig, E.)

Tissue Preparation

The Rhesus macaque tissue shipped to University of California San Diego from University of California Davis consisted of the brain, brainstem, and spinal cord. The brain was cut into three blocks after being frozen in methylbutane cooled in dry ice. Once cut into blocks, the tissue was sectioned on a microtome into 40 µm coronal sections. Every 12th section was used for analysis, while the rest was stored at -20°C in Transfected Cell Selection Medium.

Immunofluorescent Labeling

The sections were immunohistochemically stained for Green Fluorescent Protein (GFP), while Neuronal Nuclei (NeuN). GFP labeled all cell bodies and axons infected by both gCOMET and AAV-Cre and NeuN labeled all cell bodies. First the tissue was washed three times in Tris-Buffered Saline (TBS) for ten minutes each. Then, to increase permeability to antibodies, the tissue was treated with 50% methanol diluted in TBS for 5 minutes, 100% methanol for 30 minutes, and 50% methanol a second time for 5 minutes. Sections were then washed with TBS three times for 5 minutes each. Non-specific binding was blocked with TBS plus 0.25% Triton X-100 and 5% Donkey serum (TBS++) and was left for 1 hour. The tissue was then incubated in primary antibodies against GFP (Chicken, 1:2000) and NeuN (Mouse, 1:2000) which were diluted with TBS ++ (1:2000), overnight at 4°C, and then washed with TBS three times at 10 minutes each. Tissue was then incubated for 2 hours at room temperature with a secondary antibody containing 568 conjugated donkey anti-chicken (1:500) and 647 conjugated donkey anti-mouse (1:500) diluted in TBS ++. DAPI (4′,6-diamidino-2-phenylindole) nuclear stain (1:1000) was subsequently added for 5 minutes at room temperature, before the tissue was washed with TBS three times for 10 minutes each. Finally, the tissue was mounted onto gelatin subbed slides and coverslipped with Mowiol.

Fluorescence Microscope Imaging

Images of regions of interest (ROIs) of the Rhesus macaque were captured using a Keyence BZ-X710 All-in-One Fluorescence Microscope. Regions of interest included the

subthalamic nucleus, the thalamus, the zona incerta, the reticular tegmental pontine nucleus, the pontine grey, the caudate, the putamen, the red nucleus, and the superior colliculus. These specific regions of interest were chosen because of their known motor function relevance and for comparison to areas of import in a preliminary connectome experiment performed in rats. The regions of interest were imaged for GFP and NeuN at 20x magnification.

Photoshop Enhancement

Adobe Photoshop was utilized to enhance the cervically-projecting axons, labeled with GFP (green), from the background components such as neuronal cell bodies, labeled with NeuN (red), from the images captured with the Keyence BZ-X710 All-In-One Fluorescence Microscope. To enhance the GFP and decrease the NeuN visible, first the "Hue and Saturation" of "Yellow" was decreased to zero to remove background noise. The "Levels" feature for "RGB" and for "Green" were then increased to amplify the GFP. "Hue and Saturation" of "Red" and "Yellow" were decreased to zero to further remove background noise and the signal from the red NeuN labeling of the neuronal cell bodies. The enhancement of axons from background noise allowed for more effective quantification of the axons in subsequent stages of analysis.

Quantification of Summed Axon Length

Fiji/Image J software was utilized to analyze the Photoshopped images of the ROIs. First, the free hand tool was used to outline the ROIs on the original images captured with the Keyence BZ-X710 All-In-One Fluorescence Microscope and then stored in the ROI

Manager. The outlines of the ROIs were determined by cross referencing between online resources, Brain Maps (http://brainmaps.org) and Scalable Brain Atlas (Dubach, M.F. & Bowden, D.M., 2009), and "The Rhesus Monkey Brain in Stereotaxic Coordinates" (Paxinos, G., Huang, X. & Toga, A. W., 1999). The Photoshop enhanced images were then split into channels (Image -> Color-> Split Channels). Only the green channel images were used for further analysis to quantify the axons with GFP. The green channel images were thresholded (Image -> Adjust -> Threshold) to approximately 50/255. Thresholding the image makes the image black and white and represents the image in total pixels. Total pixel images were skeletonized (Plugins -> Skeleton -> Skeletonized 2D/3D) to convert all axon width to exactly one pixel wide. ROI outlines from the ROI Manager were then overlaid onto the skeletonized images and were measured for total area of the ROI and for the total amount of pixels within the ROI. The total amount of pixels in the ROI were recorded as a decimal so that they could be multiplied to the total area of the ROI as a percentage, and then multiplied by 12 (the sections analyzed are 1 in 12) to account for the complete area represented by the section. This calculation resulted in the total area of the pixelated axons, or the total summed axon length in pixels, which was then converted to µms. The results were also calculated in total summed axon length per unit volume by first converting the total summed axon length and the total averaged area of the ROIs to μm^3 and then dividing the former by the latter. Regarding nomenclature, total summed axon length refers to the total amount of µms within the specific ROI, and total summed axon length per unit volume refers to the total μm^3s within the ROI divided by the volume of the ROI in μm^3 to correct for large area bias and is comparable to axon innervation density.

Normalization of Results

Four image stacks of the pyramid contralateral to the injected motor cortex were captured by a confocal microscope at 20x magnification with a step size of 2 µms. The pyramid was chosen for the normalization factor because all of the AAV-Cre has to come up through the pyramid as part of the CST from the spinal cord, and because the pyramid is easily anatomically defined. And this specific section of the pyramid (#42 of B2S3) was chosen due to its objectively average density of labeled cervically-projecting axons in comparison to the entirety of the sections with labeled axons. The four areas chosen for image stacks were the edge farthest from the ipsilateral pyramid, the bottom of the contralateral pyramid, the middle of the contralateral pyramid, and near the divide between the ipsilateral and contralateral pyramid, and were chosen because of their comparable axon densities.

Fiji/Image J software was utilized to count all of the axons within each of the four image stacks using the "Cell Count" plugin. To make sure that axons were not double counted, a schematic of inclusion and exclusion lines was established to define which axons should be counted per stack (Fig. 2).

The total area of the pyramid was calculated from an image of the pyramid captured by the Keyence BZ-X710 All-In-One Fluorescence Microscope at 2x magnification. The pyramid ROI was hand drawn onto the image and measured for total area in pixels and then converted to µms. The conversion unit for converting pixels to µms was established by utilizing accepted scale bars in µms and the "Set Scale" function (Analyze -> Set Scale) in Image J to determine the corresponding number of equivalent pixels to µms. The area of the pyramid in µms was then multiplied by the average total number of axons in the pyramid

divided by the area of the field of view of the confocal microscope in µms, which culminated in a value of 1245.3 axons as the normalizing factor. Results in total summed axon length in µms and in total summed axon length per unit volume were then divided by this normalizing factor to calculate the normalized results. The calculated results for both total summed axon length and total summed axon length per unit volume were normalized for comparison to results in subsequent Rhesus macaque connectome projects.

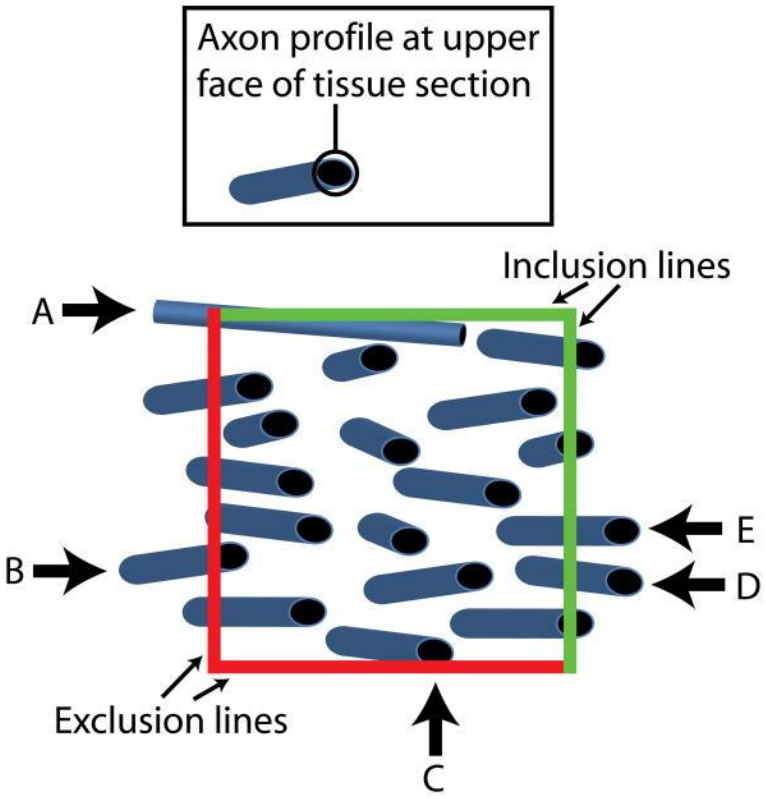

Figure 2.

Modified stereological axon quantification method. Black ovals represent axon profiles at the upper face of the tissue section, and blue cylinders represent the remainder of each axon in the tissue section. The counting frame is bounded by green inclusion lines and red exclusion lines. The axon profiles at the upper face must fall within the counting frame or

on the inclusion lines, and not touch the exclusion lines. The five axons labeled A–E would not be counted. Axon A is not an axon of passage, because it runs primarily within the plane of section, rather than through it. Axons B and C touch the exclusion lines, while axons D and E are outside of the counting frame and do not touch the inclusion lines. (Rosenzweig, E., *et al*., 2009)

Results

Total Summed Axon Length

Pixel quantification of the skeletonized images, reported as total summed axon length in µms, revealed the greatest total summed axon length in the pontine grey, closely followed by the thalamus, with the least total summed axon length in the caudate ($F_{8, 110}$=4.326, $p<0.001$, Fig.3). The red nucleus, reticulotegmental pontine nucleus, and the zona incerta also had substantial axon presence, while the subthalamic nucleus, superior colliculus, putamen, and caudate contained the least amount of axon length. Most notably, the pontine grey and the thalamus significantly differed in total summed axon length from the caudate and the putamen, and the pontine grey significantly differed from the superior colliculus (Fig. 4).

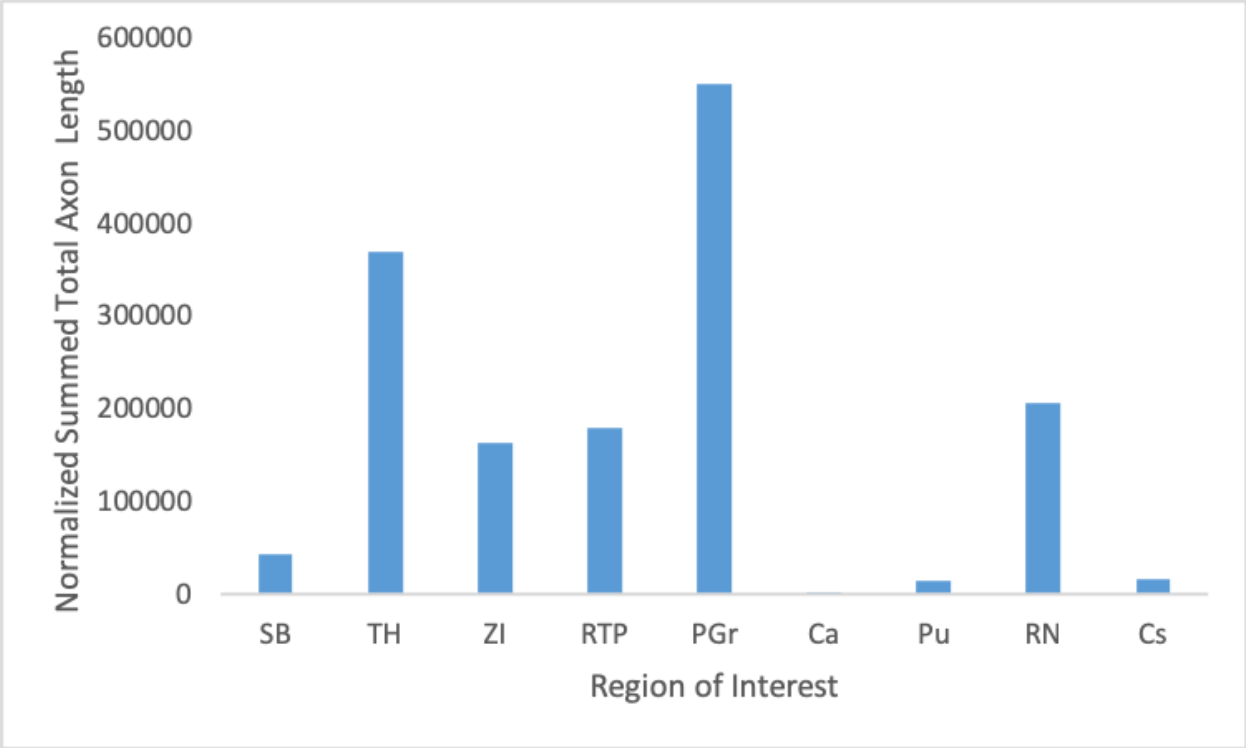

Figure 3.

Total summed axon length quantifications in the subthalamic nucleus (SB), thalamus (TH), zona incerta (ZI), reticulotegmental pontine (RTP), pontine grey (PGr), caudate (Ca), putamen (Pu), red nucleus (RN), and superior colliculus (Cs), normalized by a factor derived from the ipsilateral pyramid of the motor cortex. Bar heights represent total summed axon length sums within each region of interest.

ROIs	p adjusted
Cs-Ca	1
PGr-Ca	0.0015206
Pu-Ca	1
Rn-Ca	0.2259519
RTP-Ca	0.7185368
SB-Ca	0.9988945
TH-Ca	0.0076559
ZI-Ca	0.6991954
PGr-Cs	0.033043
Pu-Cs	1
Rn-Cs	0.497037
RTP-Cs	0.9247492
SB-Cs	0.9999101
TH-Cs	0.0656943
ZI-Cs	0.906634
Pu-PGr	0.0078569
Rn-PGr	0.9960084
RTP-PGr	0.54658
SB-PGr	0.4377099
TH-PGr	1
ZI-PGr	0.6925181
Rn-Pu	0.3491581
RTP-Pu	0.8445841
SB-Pu	0.9996868
TH-Pu	0.023669
ZI-Pu	0.8222903
RTP-Rn	0.9922208
SB-Rn	0.9300389
TH-Rn	0.997013
ZI-Rn	0.9973686
SB-RTP	0.9996281
TH-RTP	0.6498636
ZI-RTP	1
TH-SB	0.5041943
ZI-SB	0.9991241
ZI-TH	0.766502

Figure 4.

The adjusted p-values of cross comparisons of total summed axon length in regions of interest (ROIs) from a One Way ANOVA Tukey's HSD post hoc test. The regions of interest include the subthalamic nucleus (SB), thalamus (TH), zona incerta (ZI), reticulotegmental pontine (RTP), pontine grey (PGr), caudate (Ca), putamen (Pu), red nucleus (RN), and superior colliculus (SC). Adjusted p-values in red are less than 0.05.

Total Summed Axon Length Per Unit Volume

Pixel quantification results were converted to total summed axon length per unit volume to correct for an area bias, which is most prominently visible in the thalamus and subthalamic nucleus ($F_{8, 110}$=4.524, $p<0.001$, Fig. 5). The thalamus, which has the greatest total area of all the ROIs, experienced depressed representation of total summed axon length per unit volume compared to total summed axon length, while the subthalamic nucleus experienced inflated representation of total summed axon length per unit volume compared to summed total axon length (Fig. 5). Other ROIs also experienced changes in representation, such as the reticulotegmental pontine nucleus, zona incerta, and red nucleus which became comparatively inflated, while the caudate and putamen remained relatively the same. Also important to note is that the pontine grey, which reveals the greatest total summed axon length per unit volume, significantly differs from the caudate, superior colliculus, and putamen (Fig. 6).

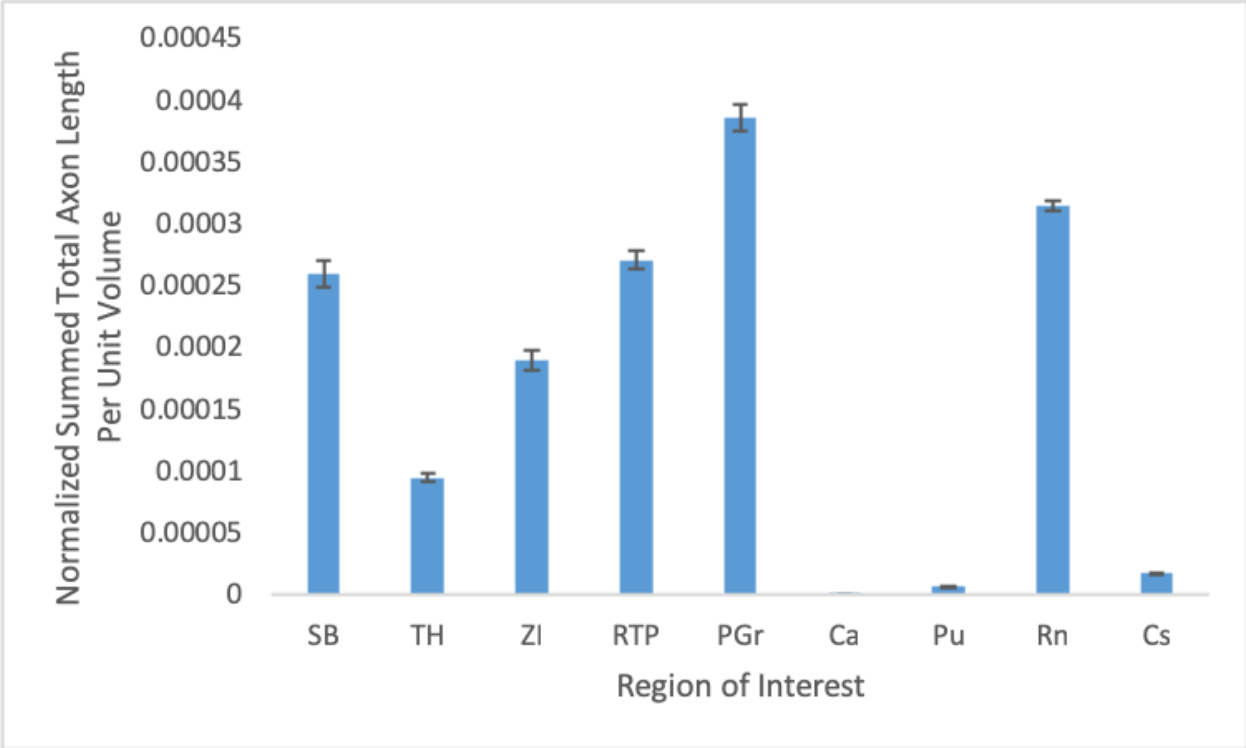

Figure 5.

Total axon density quantifications in the subthalamic nucleus (SB), thalamus (TH), zona incerta (ZI), reticulotegmental pontine (RTP), pontine grey (PGr), caudate (Ca), putamen (Pu), red nucleus (RN), and superior colliculus (Cs), normalized by a factor derived from the ipsilateral pyramid of the motor cortex. Bar heights and error bars represent means +/- se.

ROIs	p adjusted
Cs-Ca	1
PGr-Ca	0.0004176
Pu-Ca	1
Rn-Ca	0.0801625
RTP-Ca	0.0972436
SB-Ca	0.4708847
TH-Ca	0.9858589
ZI-Ca	0.595008
PGr-Cs	0.0140816
Pu-Cs	1
Rn-Cs	0.2596162
RTP-Cs	0.3481708
SB-Cs	0.696475
TH-Cs	0.9988379
ZI-Cs	0.8510935
Pu-PGr	0.002304
Rn-PGr	0.9992478
RTP-PGr	0.9591013
SB-PGr	0.9851284
TH-PGr	0.0964421
ZI-PGr	0.6060336
Rn-Pu	0.1387242
RTP-Pu	0.1814801
SB-Pu	0.5651053
TH-Pu	0.9943327
ZI-Pu	0.7166675
RTP-Rn	0.999987
SB-Rn	0.9999833
TH-Rn	0.6407209
ZI-Rn	0.9810253
SB-RTP	1
TH-RTP	0.7803646
ZI-RTP	0.9980858
TH-SB	0.9482772
ZI-SB	0.9998678

Figure 6.

The adjusted p-values of cross comparisons of axon density in regions of interest (ROIs) from a One Way ANOVA Tukey's HSD post hoc test. The regions of interest include the subthalamic nucleus (SB), thalamus (TH), zona incerta (ZI), reticulotegmental pontine (RTP), pontine grey (PGr), caudate (Ca), putamen (Pu), red nucleus (RN), and superior colliculus (SC). Adjusted p-values in red are less than 0.05.

Results Overview

Discrepancy between the quantification results of the normalized total summed axon length and the normalized total summed axon length per unit volume illuminates the importance of correcting for the large area bias of the ROIs. For this reason, the normalized total summed axon length per unit volume was chosen over normalized total summed axon length to compare to the rat connectome data with greater accuracy. Using the normalized total summed axon length per unit volume quantification results for comparison is also beneficial because of the ability to calculate variance (+/- se) for the total mean axon length within each ROI, which cannot be done for total summed axon length as it reports axon length as sums as opposed to means.

Discussion

Comparison of normalized total summed axon length per unit volume in the Rhesus macaque to innervation density in F344 rats revealed the importance of the Rhesus macaque connectome in achieving closer resemblance to a human model for clinical relevance due to innervation density differences in ROIs.

Both the Rhesus macaque and the rats express the greatest innervation in the pontine area (in Fig 5: Pon in rats, in Fig 3: RTP and PGr in Rhesus macaque) which is critical in hand movement as it relays information from the motor cortex to the cerebellum for intended contralateral movements of the arm and leg as part of the corticocerebellar pathway (Apps, *et al.*, 2018)- making it credible that both the monkey and the rats would have the greatest innervation density in this area. Further highlighting the pontine area's importance in hand function, sub-optimal functioning of the pons following a pontine based infarction

causes symptoms including ataxic hemiparesis and dysarthria-clumsy hand syndrome due to the pontine's role in informational relay within motor movements to the hand (Kim, Lee, Im, & Lee, 1995).

Beyond the pontine area, innervation densities within the Rhesus macaque and the rats differ in subsequent ROI quantities of innervation. In the monkey, the next greatest area of innervation after the pontine area is the red nucleus (in Fig 3 and 5: both RN). The rats also have slightly above moderate innervation in the red nucleus, but is just not as dense compared to other innervated regions. The red nucleus is involved in motor control via being a relay center from the motor cortex to the cerebellum, but is thought to have varying roles within motor function in different animals, most notably between bipeds and quadrupeds. In quadrupeds, such as rats and monkeys, both the parvocellular red nucleus and magnocellular red nucleus are fully developed, while in bipeds, like humans, the parvocellular red nucleus is well developed while the magnocellular red nucleus is believed to be relatively vestigial (In this study, the parvocellular red nucleus and magnocellular red nucleus are quantified together as the red nucleus). However, recent studies have shown that the human fetus and newborn have a well-developed semilunar magnocellular red nucleus, raising the possibility that tracts associated with this area may have played a role in the evolutionary advancement of bipedalism (Hicks & Onodera, 2012). This evolutionary hypothesis may explain the difference in innervation found in this study between rats, which are quadrupeds, and the Rhesus macaque, which are facultative bipeds.

In rats, the area with the greatest innervation density after the pontine area is the subthalamic nucleus (in Fig 5: STN in rats, in Fig 3: SB in Rhesus macaque). The subthalamic nucleus plays a large role in motor function as it is considered to be one of the

main regulators of motor function related to the basal ganglia. This is emphasized by the inhibition (in animal models) or high frequency stimulation (in humans) of the subthalamic nucleus resulting in suppression of Parkinson's symptoms including akinesia and dyskinesia (Benabid, 2003). The Rhesus macaque also has above moderate innervation in the subthalamic nucleus, but it apparently does not play as large of a role in motor function as the red nucleus. Interestingly, innervation densities of the caudate and putamen, both areas that make up the basal ganglia, are both very low in the monkey compared to the other ROIs. This low innervation of the caudate and putamen may contribute to the decreased innervation in the subthalamic nucleus in the monkey compared to other areas because of the subthalamic nucleus' connection with the basal ganglia for voluntary movement. Other studies confirm small amounts of innervation in the caudate, but it is surprising that the putamen has so little axon density in the Rhesus macaque given its known role in motor function and its abnormal function connection to Parkinson's disease (Künzle,1975; Brooks, 2004).

Other areas such as the thalamus (in Fig 5: VM, AV, VA/VL, Po, PF in rats, in Fig 3: TH in Rhesus macaque) and zona incerta (in Fig 3 and 5: both ZI) were comparable in the Rhesus macaque and the rats with slightly above moderate innervation density in both. The thalamus functions as a relay center for motor information to pass through to multiple motor pathways. These pathways mainly originate in areas such as the cerebellum and the basal ganglia and ascend to the primary motor cortex. Because of the thalamus' relay role in motor pathways, it makes sense as to why there is substantial innervation density within this area. The pontine area is also a relay center of motor movement, however it holds a much larger axon density than the thalamus. This may be accounted for by the pontine's location

in the brainstem, which is a necessary output area for the efferent response to the hand through the pyramids of the medulla, while the thalamus is located above the brainstem so is not as critical in the direct output of information.

The zona incerta also has high large widespread connectivity with neural centers. Its location ventral to the thalamus places it in a prime position to receive converging neural input from several major tracts to the forebrain (Watson, Lind, & Thomas, 2014). Interestingly, deep brain stimulation of the zona incerta has been shown to significantly improve Parkinson's disease symptoms, with a significant decrease in the Unified Disease Parkinson's Disease Rating Scale and adjusted “off-on” rigidity scores, better than deep brain stimulation of the subthalamic nucleus (Plaha, Ben-Shlomo, Patel, & Gill, 2006). This may be indicative of a greater importance of the zona incerta in voluntary movement than the subthalamic nucleus, despite the greater density of axons found in the subthalamic nucleus than the zona incerta in the present study.

The superior colliculus was only observed in the Rhesus macaque and was found to have sparse innervation density. The superior colliculus is mainly associated with the optic tract and visual processes as the primary integrating center for eye movements. Innervation of this area may therefore be the result of integration of visual and motor input necessary for dexterous aim. And although not observed in the rat connectome study, it can be presumed that the rat would have greater innervation in the superior colliculus than the Rhesus macaque due to the superior colliculus being part of the neural circuit for sensorimotor information integrated from visual input and sensory information from rat whiskers (Castro-Alamancos & Favero, 2016).

In this study all axons within the ROI were quantified rather than distinguishing between axons of passage and terminating axons. Innervation is usually defined as just terminating axons, however including the axons of passage may not be that detrimental given their role in motor function, especially in areas such as the pontine area, red nucleus, and thalamus which are critical relay areas for motor function modulation, signaling, and efferent response. If deemed necessary to only quantify terminating axons in subsequent Rhesus macaques however, it may be possible by immunohistochemically staining specifically for terminal boutons or by using the confocal microscope to produce a TIF from which terminal boutons can be better discerned.

In expansion of this study, it would be informative for more ROIs to be quantified, including all of the ROIs observed in the rat study, into the spinal cord, and especially of the primary motor and primary somatosensory cortices. With the monkey brain cut into coronal sections, it was difficult to accurately identify where the primary somatosensory and primary motor cortices were located without the central sulcus visible as the identifying landmark. This may be achieved in future studies however by determining and marking the location of the central sulcus pre-sectioning. Furthermore, an overall objective of this study was to establish a protocol for quantification of innervating axons in more Rhesus macaques.

Overall, the difference in innervation densities between the monkey and the rats underlines the necessity of a larger animal model, such as the Rhesus macaque, for more accurate extrapolation onto a human model. Identification of significant ROIs involved with motor function may improve targeting of treatments and rehabilitation after human SCI, as well as provide a baseline for comparison to post SCI.

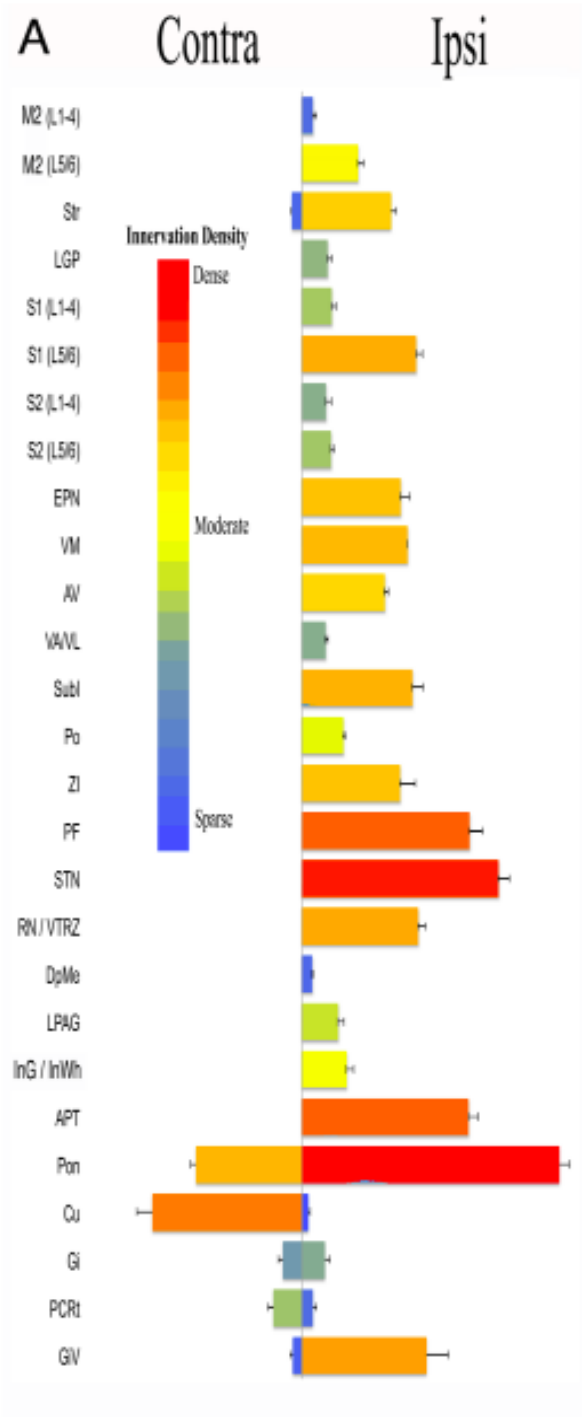

Fig 5.

Quantitative analysis of collateralization arising specifically from C8 projecting corticospinal neuron. Values shown represent the average across 4 animals +/- se (Conner,

M., Ovruchesky, E., Takashima, Y., Biane, J., Gibbs, D., & Tuskynski, M., manuscript under review).

Acknowledgements

First and foremost, I would like to express my greatest gratitude to Ephron Rosenzweig. I am thankful for his continuous support and guidance throughout my summer internship at the Mark Tuszynski Lab of the University of California San Diego and during the writing of my thesis. I would also like to thank the entirety of the Mark Tuszynski Lab for being so welcoming, and a special thank you to Janet Weber and Chase Weinholtz who took the time to instruct, inform, and mentor me throughout the research process. Thank you as well to Thomas Borowski of W.M. Keck Science who offered great advice and guidance throughout the writing of this thesis.

And of course, I would like to thank my parents, my little sisters, and my friends. My small contribution to science is framed by all the large contributions they have all made to my life.

References

Apps, R., *et al*. Cerebellar Modules and Their Role as Operational Cerebellar Processing Units. *Cerebellum* **17**, 654-682 (2018).

Benabid, A. L. Deep brain stimulation for Parkinson's disease. *Current Opinion in Neurobiology* **13**, 696-706 (2003).

BrainMaps: An Interactive Multiresolution Brain Atlas; http://brainmaps.org [retrieved on May 2018]

Brooks, D.J. Neuroimaging in Parkinson's Disease. *NeuroRx* **2**, 243-254 (2004).

Castro-Alamancos, M. & Favero, M. Whisker-related afferents in superior colliculus. *Journal of Neurophysiology* **115**, 2265-2279 (2016).

Conner, M., Ovruchesky, E., Takashima, Y., Biane, J., Gibbs, D., & Tuskynski, M. The Forelimb Corticospinal Connectome. (Manuscript under review).

Dubach, M.F. & Bowden, D.M. BrainInfo online 3D macaque brain atlas: a database in the shape of a brain. *Society for Neuroscience Annual Meeting, Chicago, IL* Abstract No. 199.5. (2009).

Hicks, T. P. & Onodera, S. The mammalian red nucleus and its role in motor systems,

including the emergence of bipedalism and language. *Progress in Neurobiology* **96,** 165–175 (2012).

Kadoya, K., et al., Spinal cord reconstitution with homologous neural grafts enables robust corticospinal regeneration. *Nature Medicine* **22**, 479–487 (2016).

Kim, J. S., Lee, J. H., Im, J. H. & Lee, M. C. Syndromes of Pontine Base Infarction. *Stroke* **26,** 950–955 (1995).

Künzle, H. Bilateral projections from precentral motor cortex to the putamen and other parts of the basal ganglia. An autoradiographic study in Macaca fascicularis. *Brain Research* **88,** 195–209 (1975).

Lang, C. & Schieber, M. Reduced muscle selectivity during individuated finger movements in humans after damage to the motor cortex or corticospinal tract. *Journal of Neurophysiology* **91**, 1722-1733 (2004)

National Spinal Cord Injury Statistical Center, Facts and Figures at a Glance. Birmingham, AL: University of Alabama at Birmingham, 2018.

Paxinos, G., Huang, X. & Toga, A. W. (1999). The Rhesus Monkey Brain in Stereotaxic Coordinates. San Diego, USA: Academic Press.

Plaha, P., Ben-Shlomo, Y., Patel, N.K., & Gill, S.S. Stimulation of the caudal zona incerta is superior to stimulation of the subthalamic nucleus in improving contralateral parkinsonism. *Brain* **129**, 1732-1747 (2006).

Rosenzweig, E., *et al*. Extensive Spinal Decussation and Bilateral Termination of Cervical Corticospinal Projections in Rhesus Monkeys. *The Journal of Comparative Neurology* **513**, 151-163 (2009).

Rosenzweig, E., *et al*. Restorative effects of human neural stem cell grafts on the primate spinal cord. *Nature Medicine* **24**, 484–490 (2018).

Watson, C., Lind, C., & Thomas, M. The anatomy of the caudal zona incerta in rodents and primates. *Journal of Anatomy* **224**, 95-107 (2014).